Submicron Spatial Modulation of an Interatomic Interaction in a Bose-Einstein Condensate

Rekishu Yamazaki,[1,2] Shintaro Taie,[1] Seiji Sugawa,[1] and Yoshiro Takahashi[1,2]

[1]*Graduate School of Science, Kyoto University, Kitashirakawa Oiwake-cho, Sakyo-ku, Kyoto, 606-8502, Japan*
[2]*JST-CREST, 4-1-8 Honmachi, Kawaguchi, Saitama 331-0012, Japan*
(Received 18 May 2010; published 30 July 2010)

We demonstrate submicron spatial control of interatomic interactions in a Bose-Einstein condensate of ytterbium (Yb). A pulsed optical standing wave, tuned near an optical Feshbach resonance, varies the *s*-wave scattering length continuously across the standing wave pattern. The modulated mean-field energy with a spatial period every 278 nm is monitored by a diffraction pattern in a time-of-flight image. We observe a wide scattering length control of up to 250 nm. The demonstrated spatial modulation of the scattering length proves that high resolution control of atomic interactions is possible.

Tunability of interatomic interactions using Feshbach resonance methods [1] has opened up a variety of possibilities in the study of ultracold quantum gases such as the formation of ultracold molecules [2], a Bose-Einstein condensate (BEC) to a Bardeen-Cooper-Schrieffer crossover with fermionic gases [3], simulation of a supernova (Bose nova) [4], and Efimov trimer states [5]. In these studies, the Feshbach resonances are induced by magnetically tuning the hyperfine energy level of a bound state to the vicinity of the incoming scattering state. The length scale for application of the Feshbach field has, so far, been much larger than the size of the atomic sample.

Many interesting experiments such as a sonic analogue of black holes [6], quantum simulation of a novel Hubbard model [7,8], and unusual Bose-nova phenomena [9] could be explored with spatial modulation of the interatomic interaction on short length scales. An alternative approach, an optical Feshbach resonance (OFR), utilizing optical coupling between bound and scattering states [10], is a promising technique for providing this possibility. With OFR methods, the intensity and the detuning of the coupling laser are used to control the scattering length [11]. Fine modulation of laser intensity by using optical standing wave and holographic techniques is routinely shown in other applications [12,13], and these techniques combined with OFR should realize the fine spatial modulation of the scattering length. The inherent nature of the optical control also enables fast manipulation; moreover, optical transitions can be found in almost any state, and control is possible for numerous situations and atomic species.

Important progress along this direction has been reported in Ref. [14], where successful control of a magnetic Feshbach resonance of alkali-metal atoms with a laser light was demonstrated. Fine spatial control of the scattering length has, however, not yet been demonstrated, so far. In this Letter, we report our successful demonstration of OFR modulation of the *s*-wave scattering lengths on the scale of hundreds of nanometers.

For the demonstration of submicron control of the scattering length, we apply a pulsed optical standing wave to a BEC of ytterbium (^{174}Yb) atoms. The pulsed light for OFR is tuned to the vicinity of the weak intercombination $^1S_0$-$^3P_1$ photoassociation resonances with the resonant wavelength of 556 nm, which results in a modulation of the mean-field energy of the condensate with a spatial period of 278 nm. The resulting phase modulation of the condensate is observed in the diffraction pattern in time-of-flight (TOF) images. The observed behavior is well explained by the semiclassical theory of Bohn and Julienne [15]. Our analysis shows scattering length variation of up to 250 nm over a (comparable) distance of only ~280 nm.

To determine the expected change of scattering length a and photoassociation rate K due to the applied laser field, the formalism of Bohn and Julienne is valid under our conditions. In their formalism, both parameters can be calculated in terms of the radiative decay rate of molecule γ, the light-induced width Γ, and the detuning of the OFR laser from a photoassociation resonance Δ. The energy level diagrams relevant to this work is shown in Fig. 1(b). The light-induced width Γ is given by $\Gamma(I) = 3I\gamma\lambda^3 f_{\rm rot} f_{\rm FC}/8\pi c$, where $f_{\rm rot} = 1/3$ is the rotational factor for the relevant transition, $f_{\rm FC}$ is the Frank-Condon factor, c is the speed of light in a vacuum, and $\lambda = 555.8$ nm and I are the wavelength and the intensity of the OFR laser, respectively. For the weak excitation regime, where $\Gamma \ll \gamma$, the scattering parameters are given by

$$a = a_{bg} + \delta a = a_{bg} + \frac{1}{2k}\frac{\Gamma\Delta}{\Delta^2 + \gamma^2/4}, \qquad (1)$$

$$K = \frac{\pi\hbar}{\mu k}\frac{\Gamma\gamma}{\Delta^2 + \gamma^2/4}, \qquad (2)$$

where $a_{bg} = 5.55$ nm is the background *s*-wave scattering length of ^{174}Yb, $\mu = m/2$ is the reduced mass of two scattering atoms with mass m, and $k = \sqrt{21/8}\frac{1}{2R_{\rm TF}}$ is the wave number calculated from the momentum of the condensate with Thomas-Fermi radius $R_{\rm TF}$ [16]. δa is the variation of the scattering length due to the OFR and is proportional to I.

Despite its potentially wide applicability, the use of OFR has been scant [11]. One reason for this is that usually the optical coupling also induces inelastic scattering, leading to rapid atom depletion. The use of narrow transitions in alkaline-earth-metal-like atoms [17] to avoid inelastic scattering loss was successfully demonstrated in a recent experiment in our group by using the $^1S_0$-$^3P_1$ intercombination transition in thermal gases of ^{172}Yb and ^{176}Yb [18].

In that earlier work, a relatively low inelastic scattering rate was observed, an order of magnitude less than the case of alkaline atoms, indicating the possibility of observing large tunings of scattering length over short distances, as we report here. In this work we extend this technique to a condensate of ^{174}Yb.

To demonstrate the capability of OFR to modulate the s-wave scattering length on short length scales and also on short time scales, we use a pulsed optical lattice beam as the OFR light, as shown in Fig. 1(a). The application of a pulsed optical lattice beam generally results in a diffraction of a released BEC, which was previously studied both theoretically and experimentally [12]. In a phase modulation regime, where the exposure time of the optical lattice τ is much smaller than the minimum classical oscillation period of the formed lattice, the effect of the lattice is treated as a thin grating. The phase of the condensate modified by the lattice has the form

$$\phi(z) = \frac{U(z)\tau}{\hbar}, \quad (3)$$

with $U(z) = U_0\cos^2(qz)$, where q is the wave number of the lattice laser and z is the direction along the lattice laser propagation. The potential U_0 experienced by the atoms in the ground state at an antinode of the optical lattice is given by

$$U_0 = \frac{\hbar\Omega^2}{\Delta_{\text{atom}}} + \frac{4\pi\hbar^2 n_a}{m}\delta a. \quad (4)$$

The first term describes the atomic light shift, where Ω and Δ_{atom} correspond to the Rabi frequency and the detuning of the OFR laser to the atomic excited state, respectively. The second term represents the OFR-induced shift of the mean-field energy and thus is proportional to the scattering length variation δa and the atom density n_a. It is noted that there is a mean-field energy $U_{\text{MF}} = \frac{4\pi\hbar^2 n_a}{m}a_{bg}$ across the condensate. However, it is not susceptible to the OFR laser and does not contribute to the diffraction pattern. It is clear from Eqs. (1) and (4) that the OFR dispersively varies the scattering length, and therefore the mean-field energy, across a photoassociation resonance. From the diffraction pattern of the condensate generated from the phase modulation $\phi(z)$ imparted by the OFR, one should be able to extract the variation of the scattering length.

The method for the all-optical formation of the ^{174}Yb condensate is described in Ref. [19]. After the evaporation in a crossed far-off resonant trap, an almost pure ^{174}Yb condensate is prepared with an atom number of up to 1.5×10^5 in a typical harmonic trap potential $(\omega_x, \omega_y, \omega_z) = 2\pi \times (32, 121, 199)$ Hz with corresponding Thomas-Fermi radii of $(15.7, 4.2, 2.5)$ μm. A simple schematic of the experimental process after the preparation of condensate is shown in Fig. 1(a). Following the condensate formation, we release the condensate from the trap by turning off the far-off resonant trap lasers. At the release, the OFR laser pulse of a 1D optical lattice is turned on for several microseconds with a typical power of 1–100 μW with a beam radius $w = 70$ μm at the location of the condensate. The OFR laser is tuned near the $^1S_0$-$^3P_1$ photoassociation resonances with the vibrational quantum numbers $v' = 11$, 12, and 13, which correspond to the detuning Δ_{atom} of -69, -117, and -192 MHz, respectively [20]. After a TOF time of typically 10 ms, the absorption image is taken for the diffraction pattern analysis. For every OFR pulse, the power of the pulse is monitored by a fast photodiode and recorded with an oscilloscope to compensate for the power instability.

A typical image and a column density of the obtained diffraction pattern are shown in Figs. 1(c) and 1(d), respectively. Each peak in the image represents the momen-
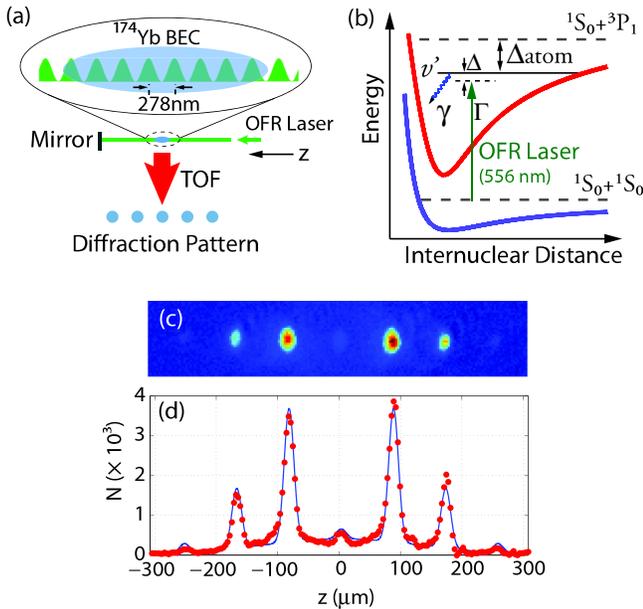

FIG. 1 (color online).   (a) Schematic of the experimental setup. A ^{174}Yb condensate is irradiated with the standing wave formed by an OFR laser. The diffraction pattern in the TOF image is observed. (b) Energy diagram of the relevant states for the experiment. The $^1S_0$-$^3P_1$ photoassociation transitions to the vibrational states $v' = 11$, 12, and 13 are used for the OFR. (c) Typical diffraction pattern obtained in the experiment. Each peak in the image represents different momentum components imparted by the pulsed lattice. (d) An integrated column density of the image where the red dots and a blue line correspond to the data and the fitted line for the determination of β, respectively.

tum component $p_n = n2\hbar q$ ($n = 0, \pm 1, \pm 2, \dots$) imparted by the pulsed lattice. Population distribution for each momentum state is described as $P_n = J_n^2(\beta)$, where $\beta = U_0\tau/2\hbar$ and $J_n(z)$ are Bessel functions of the first kind [12]. For the image analysis, we first sum the image along the vertical axis to obtain an integrated column density profile in the horizontal axis and fit the density profile by the Bessel functions to obtain the modulation index β. Each peak is convoluted with a Gaussian function to account for the momentum spread and the finite image resolution. It is also noted that we subtract the background distribution in the images. There are two origins of the background distribution: the residual thermal component and the elastic scattering of wave packets of condensate with different momentum during the TOF [21,22]. Strictly speaking, the atom distributions from the later phenomena are non-Gaussian. However, due to low atom counts from the elastic scattering we do not observe clear deviation from the Gaussian fit for the background distribution.

The images of the diffraction pattern across the photoassociation resonances are collected by scanning the OFR laser frequency. We keep the OFR pulse length short, and all the diffraction pattern images collected are in the phase modulation regime. Shown in Fig. 2 are the typical β and atom number after the OFR pulse as obtained from the images. The observed β has a dispersive shape centered at the photoassociation resonance, where atom loss is maximum. The slight increase in β towards the atomic resonance is due to the variation of the atomic light shift. To extract the scattering length from the data, we first fit the observed β to determine Γ and Ω. We then calculate the atom loss and the variation of the scattering length δa from these parameters. Atom loss obtained from the data agrees well with that obtained from the fit to the β variation.

The clear dispersive variation in β is direct evidence of the OFR effect. We further investigate the behavior of the signals to confirm the OFR effect. First, the variation of δa with respect to the OFR laser power is measured. The fact that $\Gamma/2\pi < 20$ kHz for all the data obtained means that
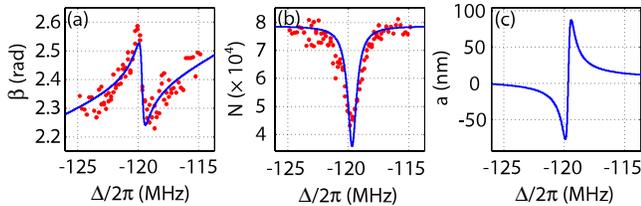
all the measurements are performed in the weak excitation condition $\Gamma \ll \gamma$ ($= 2\pi \times 364$ kHz) where δa should be proportional to the laser intensity as shown in Eq. (1). The results shown in Fig. 3(a) clearly confirm the linear dependence, which is consistent with the weak excitation regime. The observed variation of the scattering length up to 250 nm is quite large. A larger variation could be achieved with a higher laser power; however, the increased photoassociative atom loss diminishes the diffraction signal, which limited our measurement with the current power. It is important to note that δa varies continuously from the antinode, where the effect of OFR is maximum, to the node where the effect of OFR is absent. The OFR laser wavelength of $\lambda = 555.8$ nm results in a periodic modulation of δa in approximately 278 nm spacing.

Second, the variation of the modulation index across the photoassociation resonance $\delta\beta$ with respect to the atom number is measured. The OFR effect is proportional to the density as is shown in Eq. (4). For a given trap frequency, the density n_a is proportional to $N^{2/5}$ [23]. Figure 3(b) shows the variation of $\delta\beta$ as a function of the atom number with a best fit curve of N^p shown with a blue line. From the best fit, we obtain $p = 0.41$, and the value agrees well with the $N^{2/5}$ dependence predicted. The agreement between the data and the curve clearly shows that the observed $\delta\beta$ comes from the mean-field energy of the condensate.

The effect of the OFR depends on the Frank-Condon factor of the photoassociation resonance chosen. From the same measurement on different photoassociation resonances, we obtain the optical length defined as $L_{\mathrm{opt}} = \Gamma/2k\gamma$, which describes the strength of the OFR coupling for each resonance. We plot the optical length obtained from the measurement (blue dots) and the numerical calculation (red dots) [24] in Fig. 4. The error bar in the figure shows the uncertainty of L_{opt}, estimated from the uncer-

FIG. 2 (color online).   (a) Observed modulation index β at $v' = 12$ transition. The OFR laser power and pulse duration used are 26 μW and $\tau = 8$ μs, respectively, with atom number $N = 1.0 \times 10^5$. (b) Number of atoms remained after the OFR pulse, and (c) calculated scattering length. We first fit the variation of β by using the formalism by Bohn and Julienne to determine light-induced width Γ. Blue lines in (b) and (c) are calculated atom loss and scattering length variation by using the Γ obtained from the fit in (a), respectively.
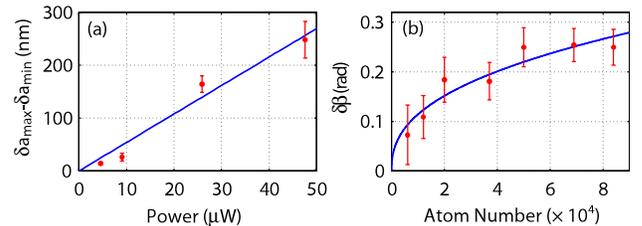
FIG. 3 (color online).   (a) Power dependence of the scattering length variation along with a linear fit line. The linear dependence is consistent with the weak excitation expected from the Γ value obtained from the data. The OFR laser pulse duration of 5–30 μs are used for different laser power. (b) Atom number dependence of $\delta\beta$ along with the best fitted curve in blue. The OFR laser power of 33 μW is used. From the fit, we obtained $p = 0.41$ ($\sim 2/5$) for N^p dependence fitting, which agrees well with the predicted density dependence. Both data in (a) and (b) are obtained at $v' = 12$ transition. The error bars in the figures show the root mean squared error of the data obtained from the fitting procedure of the modulation index β.
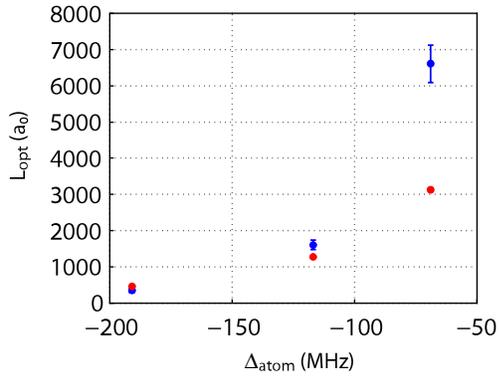
FIG. 4 (color online). Comparison between calculated (red dots) and measured (blue dots) L_{opt}. The rapid increase of L_{opt} for the shallower detuning is observed for both results. Part of the discrepancy between two results may be due to the uncertainty in the laser intensity estimation at the condensate.

tainty of the fitting of β. As the transition gets shallower toward the atomic resonance, the measured optical length shows faster increase in the optical length than the numerically calculated values. The tendency in the variation of L_{opt}, however, is consistent between two results. Part of the discrepancy may be due to the uncertainty in the fitting of β and the laser waist estimation error of up to 10% at the condensate; however, this is not enough to fully explain the large discrepancy at the shallow resonance. Clarifying the origin of this discrepancy is an interesting future work.

In conclusion, we demonstrate rapid, submicron modulation of the scattering length by using optical Feshbach resonances in a ^{174}Yb condensate. A large scattering length variation of up to 250 nm is obtained with a spatial modulation of 278 nm by observing a diffraction pattern in a time-of-flight image. The demonstrated fine spatial modulation of the scattering length opens up a wide variety of applications. New applications may benefit not only from the fine spatial resolution offered by a OFR but also the inherently available fast manipulation [25]. The time constant for the manipulation of the OFR can be quite fast compared to the magnetic Feshbach resonances and could be used to control and study the nonequilibrium dynamics of the condensate. In addition to these possibilities, creation of multiple frequency superlattices with frequency components tuned to different OFR resonances may create intricate patterns of large variation in the interaction strength. Independent control of different scattering lengths [26] and local manipulation of the condensate or the condensate in the lattices may also be possible.

[1] S. Inouye *et al.*, Nature (London) **392**, 151 (1998).
[2] C. A. Regal *et al.*, Nature (London) **424**, 47 (2003).
[3] M. Bartenstein *et al.*, Phys. Rev. Lett. **92**, 203201 (2004).
[4] J. L. Roberts *et al.*, Phys. Rev. Lett. **86**, 4211 (2001).
[5] T. Kraemer *et al.*, Nature (London) **440**, 315 (2006); G. Barontini *et al.*, Phys. Rev. Lett. **103**, 043201 (2009); J. R. Williams *et al.*, Phys. Rev. Lett. **103**, 130404 (2009).
[6] L. J. Garay, J. R. Anglin, J. I. Cirac, and P. Zoller, Phys. Rev. Lett. **85**, 4643 (2000).
[7] X. L. Deng, D. Porras, and J. I. Cirac, Phys. Rev. A **77**, 033403 (2008).
[8] F. K. Abdullaev, A. Gammal, M. Salerno, and L. Tomio, Phys. Rev. A **77**, 023615 (2008).
[9] G. J. Dong, B. B. Hu, and W. P. Lu, Phys. Rev. A **74**, 063601 (2006).
[10] P. O. Fedichev, Y. Kagan, G. V. Shlyapnikov, and J. T. M. Walraven, Phys. Rev. Lett. **77**, 2913 (1996).
[11] M. Theis *et al.*, Phys. Rev. Lett. **93**, 123001 (2004).
[12] Y. B. Ovchinnikov *et al.*, Phys. Rev. Lett. **83**, 284 (1999).
[13] J. Sebby-Strabley, R. T. R. Newell, J. O. Day, E. Brekke, and T. G. Walker, Phys. Rev. A **71**, 021401(R) (2005).
[14] D. M. Bauer *et al.*, Nature Phys. **5**, 339 (2009).
[15] J. L. Bohn and P. S. Julienne, Phys. Rev. A **60**, 414 (1999).
[16] J. Stenger *et al.*, Phys. Rev. Lett. **82**, 4569 (1999).
[17] R. Ciuryło, E. Tiesinga, and P. S. Julienne, Phys. Rev. A **71**, 030701(R) (2005).
[18] K. Enomoto, K. Kasa, M. Kitagawa, and Y. Takahashi, Phys. Rev. Lett. **101**, 203201 (2008).
[19] Y. Takasu *et al.*, Phys. Rev. Lett. **91**, 040404 (2003).
[20] S. Tojo *et al.*, Phys. Rev. Lett. **96**, 153201 (2006).
[21] Y. B. Band, M. Trippenbach, J. P. Burke, and P. S. Julienne, Phys. Rev. Lett. **84**, 5462 (2000).
[22] A. P. Chikkatur *et al.*, Phys. Rev. Lett. **85**, 483 (2000).
[23] C. J. Pethick and H. Smith, *Bose-Einstein Condensation in Dilute Gases* (Cambridge University Press, Cambridge, England, 2002).
[24] M. Borkowski *et al.*, Phys. Rev. A **80**, 012715 (2009).
[25] K. Staliunas, S. Longhi, and G. J. de Valcárcel, Phys. Rev. Lett. **89**, 210406 (2002); H. Saito and M. Ueda, Phys. Rev. A **70**, 053610 (2004).
[26] P. Zhang, P. Naidon, and M. Ueda, Phys. Rev. Lett. **103**, 133202 (2009).